Many-body definition of a Fermi surface: Application to angle-resolved photoemission

Th. Straub, R. Claessen, P. Steiner, and S. Hüfner
Fachbereich Experimentalphysik, Universität des Saarlandes, D-66041 Saarbrücken, Germany

V. Eyert
Hahn-Meitner-Institut, Glienicker Straβe 100, D-14109 Berlin, Germany

K. Friemelt and E. Bucher
Fakultät für Physik, Universität Konstanz, D-78434 Konstanz, Germany
(Received 12 February 1997)

In real metals with interacting conduction electrons a Fermi surface (FS) can no longer be defined as separating occupied from unoccupied one-electron states in **k** space, but is rather given by the location of discontinuities in the momentum distribution function $n(\mathbf{k})$. Here we show that this many-body theoretical definition provides a valuable prescription for FS measurements by angle-resolved photoemission, which compared to conventional FS mapping not only extends the method to metals with extremely narrow bands, but also enhances its precision in the application to wide band systems. We demonstrate this on $TiTe_2$ and Cu(001) as test cases. [S0163-1829(97)00820-5]

The knowledge of the Fermi surface (FS) is a crucial prerequisite for understanding the electronic properties of a metal.[1] The standard method of measuring the FS is based on the de Haas-van Alphen (dHvA) effect[2] and determines the external cross-sectional area of the FS in a plane normal to an applied magnetic field. During the last few years a method based on angle-resolved photoemission spectroscopy (ARPES) has been established[3–5] that is capable of giving a *direct image* of two-dimensional FS cross sections. Here, photoelectrons originating from a small energy window centered at the Fermi level are measured as a function of the emission angle, i.e., as a function of the wave vector **k**. When a conduction band crosses the Fermi energy, and hence the detection window, it will give rise to an intensity maximum, whose location is identified with the Fermi vector $\mathbf{k_F}$. Measuring the photoelectrons over the entire half space above the sample surface[3–5] thus yields a map of the FS contour in the **k**-space surface probed with a given photon energy. This interpretation of the experiment is based on the usual one-electron band picture in which the FS separates occupied from unoccupied states in **k** space.

Difficulties can arise in the case of narrow band systems, i.e., if the bandwidth is not large or even smaller than the detection energy window. As we will show below, the measured intensity maximum will then be off the true FS. Furthermore, in these materials the band narrowing is often caused by strong correlation effects, which make the picture of a one-electron band crossing the Fermi level and changing from occupied to unoccupied highly questionable. Here we present a method that solves both problems by utilizing the many-body theoretical generalization of the FS concept to Fermi liquid systems, in which the Fermi vectors are defined by the location of discontinuities in the momentum distribution $n(\mathbf{k})$.[6] This approach not only allows us to extend the FS mapping technique to materials with strongly interacting electrons, but also leads to less stringent requirements on energy resolution.

We demonstrate the usefulness of this method by application on Cu and 1T-$TiTe_2$. While Cu is a conventional three-dimensional metal, $TiTe_2$ crystallizes in the layered 1T-CdI_2 structure and has quasi-two-dimensional electronic properties. Its (semi)metallic behavior results from an overlap of Te $5p$ and Ti $3d$-derived bands. As we have demonstrated earlier, $TiTe_2$ is an ideal reference material for electron-spectroscopic studies of Fermi-liquid behavior.[7–10] Besides dimensionality, both materials differ strongly in their conduction-band widths. Whereas the sp-band of Cu shows large free-electron-like dispersions, the Ti $3d$ band of $TiTe_2$ is very narrow with an occupied bandwidth of only $\sim$100 meV.[7]

The experiments have been performed with a VG ESCALAB Mk. 2 spectrometer equipped with a two-axis manipulator that allows computer-controlled sample rotation.[11] The data presented here were obtained at room temperature with He-I radiation ($h\nu = 21.2$ eV) and a width ΔE of the energy window of 100 meV. The angular resolution was $\pm 1.75°$. The location of the Fermi energy was determined by the Fermi edge of a polycrystalline In sample. The $TiTe_2$ crystals were cleaved *in situ* by knocking off a steel post glued on top of the sample. Typical sample sizes were 5×5 mm. The Cu(001) crystal (diameter $\sim$12 mm) was prepared by repeated cycles of Ar^+ sputtering and annealing. Surface quality has been checked by x-ray photoemission spectroscopy and low energy electron diffraction measurements.

The experiments are complemented with first-principles electronic band-structure calculations based on density-functional theory and the local-density approximation. As a calculational scheme we employed the augmented spherical waves (ASW) method[12] in its scalar-relativistic implementation. The calculations on $TiTe_2$ were performed in much the same way as in our previous paper.[7]

Figure 1(a) shows the intensity distribution of photoelectrons excited from the Fermi level of $TiTe_2$. The most promi-

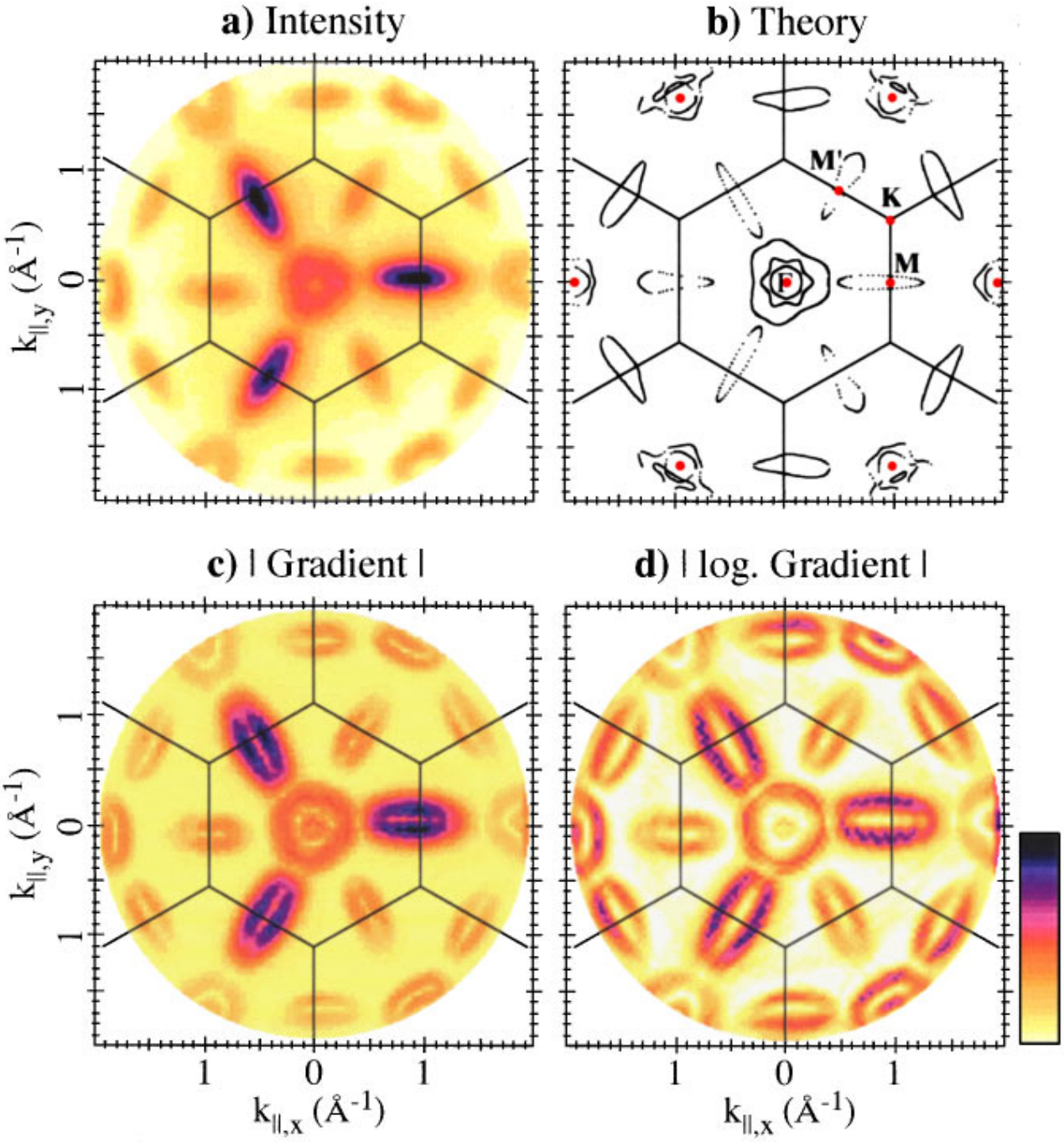

FIG. 1. (Color) (a) Photoemission intensity map $w(\mathbf{k})$ for excitations from the Fermi level of $TiTe_2$ ($h\nu = 21.2$ eV). The Brillouin zone is indicated. (b) Corresponding Fermi-surface contours obtained from an ASW band calculation. (c) Modulus of the two-dimensional gradient $|\nabla_{\mathbf{k}} w(\mathbf{k})|$ of the map in (a). (d) Modulus of the logarithmic gradient $|\nabla_{\mathbf{k}} \ln w(\mathbf{k})|$

nent features are the ''cigar-shaped'' intensity maxima centered at the M points, which originate from the Ti $3d$ band. The observed intensity pattern reflects the threefold symmetry of the crystal structure that requires a distinction between M and M' points.[7] Though the electronic band structure itself does not deviate much from sixfold symmetry in the hexagonal $1T$ structure,[7] the optical transition matrix elements are strongly affected by photoelectron diffraction off the three Te atoms sitting atop each Ti site.[13] Near the center of the Brillouin zone (BZ) three Te $5p$ bands cross the Fermi level very close to each other, giving rise to a broad intensity spot at the Γ point. Note that we can also access parts of the second BZ (in the periodic zone scheme). The identification of the intensity maxima becomes possible by comparison to conventional band mapping results[7] and to a corresponding FS cut derived from our ASW calculations [Fig. 1(b)]. Apparently, the overall shape of the measured intensity map is already in good agreement with the calculated FS topology. However, the *contours* of the Ti $3d$-derived electron pockets at the M point(s) are clearly not resolved. This is a consequence of the very narrow (occupied) width of the Ti $3d$ band. Its highest binding energy accessible by He-I radiation

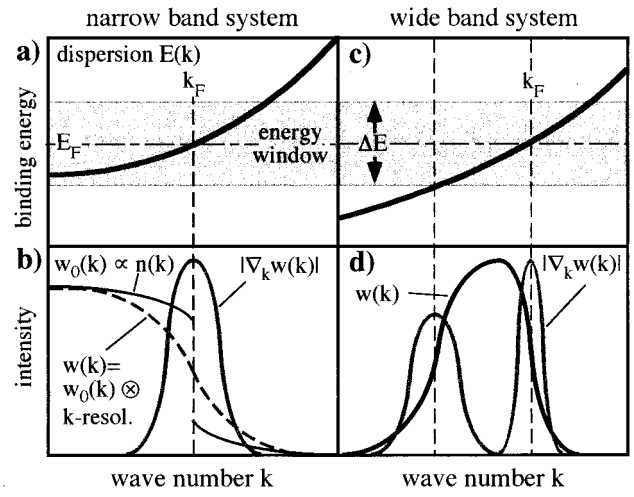

FIG. 2. Schematic representation of the integrated photoemission intensity $w(\mathbf{k})$ and its derivative for experiments on narrow band (bandwidth $\ll\Delta E$) and wide band systems (bandwidth $\gg\Delta E$). (a) Dispersion $E(\mathbf{k})$ of a narrow band. (b) Integrated intensities $w_0(\mathbf{k})$ for $T=0$ and $\Delta k=0$ (black curve) and $w(\mathbf{k})$ for $T>0$ and $\Delta k>0$ (black dashed curve). The maximum of $|\nabla_{\mathbf{k}}w(\mathbf{k})|$ (gray curve) occurs precisely at the Fermi vector. (c) Same as (a), but for a wide band. (d) Behavior of $w(\mathbf{k})$ and its derivative in the wide band case (see text for discussion).

is only 70 meV (Ref. 7) and therefore comparable with the width of the energy detection window. In this case the experimental intensity distribution $w(\mathbf{k})$ no longer represents the position of the Fermi vectors, but rather measures the integrated peak intensity and thus becomes proportional to the momentum distribution function $n(\mathbf{k})=\int_{-\infty}^{\infty}d\omega\, A(\mathbf{k},\omega)f_{\mathrm{FD}}(\omega,T)$ [where ω is the energy relative to E_F, $A(\mathbf{k},\omega)$ is the single-particle spectrum and f_{FD} represents the Fermi-Dirac distribution]. This interpretation goes well beyond the conventional independent-electron picture and assumes that the ARPES signal is proportional to $A(\mathbf{k},\omega)$.[14] While this still needs to be generally verified, many aspects of ARPES data on $TiTe_2$ are indeed found to be in excellent agreement with single-particle spectra expected from a Fermi liquid.[7–10] Furthermore, it has recently been demonstrated by ARPES on cuprate superconductors[15,16] that $n(\mathbf{k})$ is a useful quantity in the study of highly correlated metals. In general, the measured intensity distribution $w(\mathbf{k})$ is additionally modulated by a $\mathbf{k}$-dependent transition matrix element $|M_{\mathrm{if}}(\mathbf{k})|^2$, which in the case of $TiTe_2$ is responsible for the mentioned intensity differences between the M and M' points and also between the first and second BZ.

In order to extract precise Fermi-surface information from the data, we now utilize the fact that in a Fermi liquid-type metal $n(\mathbf{k})$ displays at each Fermi vector $\mathbf{k}_F$ a discontinuous step, whose size equals the quasiparticle weight factor.[6] In fact, this discontinuity marks the generalized definition of a FS in an interacting many-electron system.[6] Figures 2(a) and 2(b) give a schematic illustration of the experimental conditions for a narrow band system, where the occupied band always stays within the energy window of the experiment. For simplicity it is assumed that the transition matrix element is a slowly varying function of $\mathbf{k}$ (at least in the vicinity of $\mathbf{k}_F$) and that the used energy window is of rectangular shape. The measured intensity $w_0(\mathbf{k})$ is then proportional to $n(\mathbf{k})$ and shows at $T=0$ and for ideal $\mathbf{k}$ resolution ($\Delta k=0$) the expected discontinuity at $\mathbf{k}_F$ leads to a δ-like singularity in the modulus of the gradient $|\nabla_{\mathbf{k}}n(\mathbf{k})|$. For finite temperature T and angular resolution $\Delta\theta$ the step in the integrated intensity [shown here as $w(\mathbf{k})$] will become continuous due to an effective overall $\mathbf{k}$ broadening $\Delta\mathbf{k}$.[17] However, the maximum of $|\nabla_{\mathbf{k}}w(\mathbf{k})|$ still clearly indicates the correct location of the Fermi vector.

The application of this method to the measured intensity distribution of $TiTe_2$ is shown in Fig. 1(c), which contains a map of the (two-dimensional) gradient $|\nabla_{\mathbf{k}}w(\mathbf{k})|$. In contrast to the bare intensity data one can now identify real FS contours, especially those of the Ti $3d$ pockets at the M (M') points. Also the broad intensity spot due to the Te $5p$-derived FS sheets is resolved into two concentric contours around the Γ point. The third predicted sheet [cf. Fig. 1(b)] is not observed, but we should mention here that the situation is more complicated than for the Ti $3d$ band, due to the much larger bandwidth and the near degeneracy of the Te $5p$ bands. The map of the gradient still contains the large intensity variations present in the original data (e.g., between the M and M' points) because they are caused by the modulating matrix element that enters essentially as a factor. To a first approximation its effect can be largely suppressed by normalizing the gradient to the bare intensity distribution, i.e., by taking the *logarithmic* gradient $|\nabla_{\mathbf{k}}w(\mathbf{k})|/w(\mathbf{k})=|\nabla_{\mathbf{k}}\ln w(\mathbf{k})|$ [Fig. 1(d)]. Unfortunately, it also leads to a systematic shift of the gradient maximum towards lower $w(\mathbf{k})$ values on the scale of the Δk (the applied $\mathbf{k}$ resolution) seen, e.g., by the somewhat broader Ti $3d$ pockets. Thus, for a quantitative FS determination the use of the *bare* gradient will generally yield more precise data.

The described method is not only useful for narrow band systems, but also serves to enhance FS information on systems with large conduction-band widths (compared to ΔE), which is sketched in Figs. 2(c) and 2(d). In this case, the band will remain outside the detection window for wave vectors far from $\mathbf{k}_F$. As the band disperses towards E_F, it eventually enters the energy window resulting in a rise of the measured intensity $w(\mathbf{k})$. The signal drops again sharply at the Fermi vector when the band (or rather the quasiparticle peak) crosses the Fermi level, which is equivalent to the discontinuity in $n(\mathbf{k})$. For finite temperature and resolution the maximum of $w(\mathbf{k})$, which in the usual interpretation of this experimental technique is thought to reflect the FS, therefore, *does not occur exactly* at $\mathbf{k}_F$, but will be shifted slightly towards the ''occupied'' side. However, of the two maxima of the gradient $|\nabla_{\mathbf{k}}w(\mathbf{k})|$, the one on the ''unoccupied'' side still accurately reflects the Fermi vector. Without prior knowledge of the band structure there are two possibilities to distinguish the ''real'' maximum from the artifact:

(i) the $\mathbf{k}$ vector of the artifact depends on the width ΔE of the detection window, whereas the discontinuity always occurs at $\mathbf{k}_F$.

(ii) The maximum of $|\nabla_{\mathbf{k}}w(\mathbf{k})|$ at $\mathbf{k}_F$ is expected to be more intense because it results from the sudden loss of a δ-like quasiparticle peak, whereas the artifact results from the

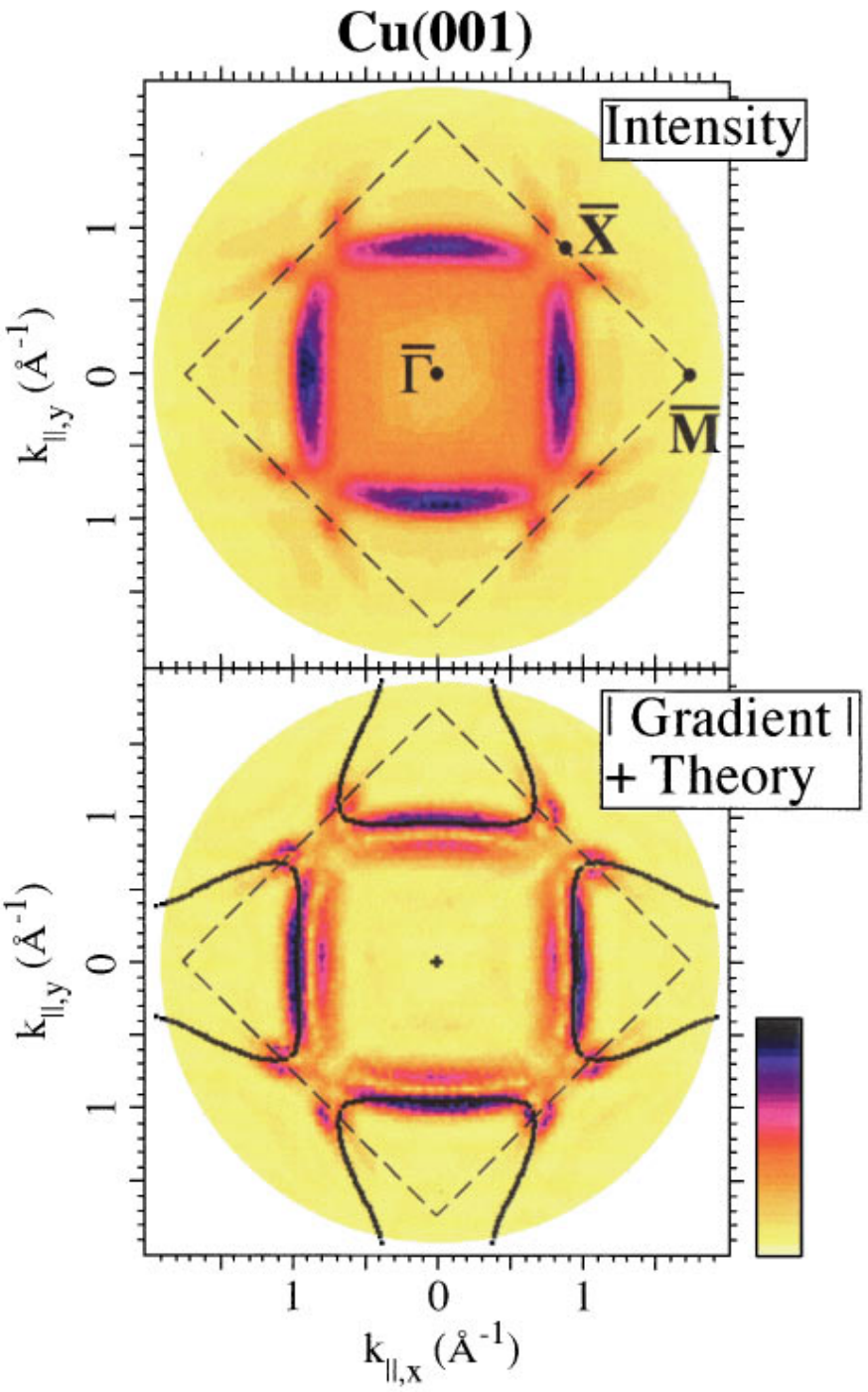

FIG. 3. (Color) Top: Fermi-level intensity map of Cu(001). The surface Brillouin zone is indicated. Bottom: Modulus of the gradient ($|\nabla_{\mathbf{k}} w(\mathbf{k})|$) of the intensity map, together with the theoretical FS contour (black line).

continuous penetration of a lifetime broadened peak into a typically Gaussian energy window, given by the instrumental response function.

This is illustrated on Cu(001) as an example. Figure 3 shows the corresponding intensity map, which agrees with that of other workers.[4] The observed pattern approximately reflects a cut through the FS of the *sp* band, which is occupied in the center of the BZ. However, a closer inspection shows that the position of the intensity maximum along the $\bar{\Gamma}$-$\bar{M}$ direction of the surface BZ *does not coincide* with an independent determination of the Fermi vector from the measured dispersion of the *sp* band (Fig. 4), as obtained from energy distribution curves on the same surface. Rather, it appears slightly shifted towards the BZ center. Also shown in Fig. 3 is the gradient $|\nabla_{\mathbf{k}} w(\mathbf{k})|$ of the intensity distribution. In line with our above discussion, we now find two sets of maxima, the outer and more intense of which is inter-

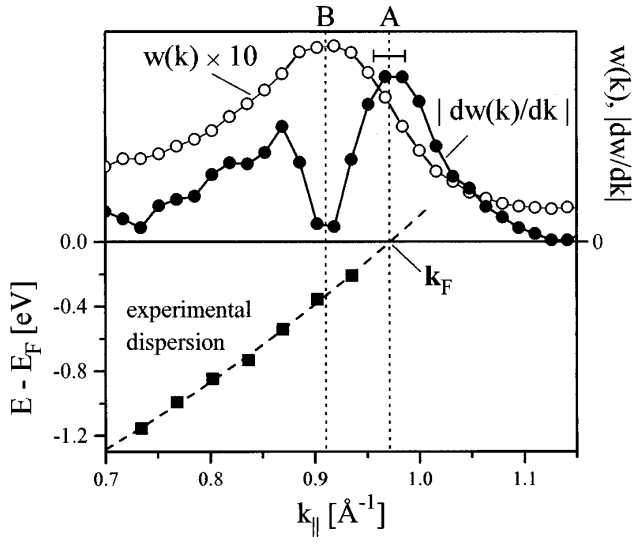

FIG. 4. Experimental dispersion of the *sp* band along the Γ-*M* azimuth of Cu(001) as obtained from energy distribution curves (squares) compared to the measured intensity $w(\mathbf{k})$ (open dots) and the modulus of its derivative (filled dots) ($\Delta\theta = \pm 0.75°$, $\Delta E = 200$ meV). Line *A* denotes the Fermi vector obtained from an extrapolation of the measured dispersion (dashed curve) that coincides very well with the maximum of $|dw(k)/dk|$. Also shown is the location of the maximum in $w(\mathbf{k})$ (line *B*).

preted as the true contour of the FS. Its positions, along Γ-*M* is now perfectly consistent with the Fermi vector obtained from the *sp*-peak dispersion. In contrast, the inner ''artifact'' contour appears slightly broader and less intense, as expected from our model. We have also calculated the FS contour with our ASW method using an inner potential of 8.5 eV relative to E_F (Ref. 18) for the relevant **k**-space cut. The theoretical FS is superimposed on the $|\nabla_{\mathbf{k}} w(\mathbf{k})|$ map of Fig. 3 and shows excellent agreement with the outer experimental contour. These results clearly demonstrate the reliability of the method presented here.

Figure 4 also illustrates the accuracy of the method. While the experimental **k** resolution[17] is reflected in the width of the structures in $|\nabla_{\mathbf{k}} w(\mathbf{k})|$, the actual uncertainty in Fermi vector determination is given by the unique identification of the maximum position (indicated by the error bar in Fig. 4) and thus much smaller than Δk. For our data analysis on Cu this amounts to an experimental uncertainty of $\sim 3\times 10^{-2}$ Å^{-1}, compared to 3×10^{-3} Å^{-1} (0.2% of the FS radius) achieved in low-temperature dHvA measurements.[19] The lower resolution of the ARPES method, however, is outweighed by a number of significant advantages. We already mentioned the direct mapping of FS contours, which with additional variation of the photon energy can be used to obtain a complete picture of the FS.[20] Furthermore and in contrast to dHvA, our method is not limited to materials with low electron scattering rates and to low temperatures, which, e.g., allows to study electronic phase transition at several hundreds K.[22]

In conclusion, we have shown that utilizing the discontinuity in the momentum distribution $n(\mathbf{k})$ not only extends the method of FS mapping by photoemission to metals with extremely narrow bands, but also enhances the precision of Fermi vector determination in the application to wide band systems. The accuracy of this method is only limited by the instrumental **k** broadening (i.e., angle resolution) and no longer by the energy resolution. This allows the use of rather large energy windows resulting in considerably higher count rates than in the conventional mode. Finally, we note that this approach is not restricted to systems with Fermi-liquid behavior, but is also applicable to more exotic many-body states such as marginal Fermi liquids or Luttinger liquids. Because some of these systems have vanishing weight at the Fermi level,[22] modulations in $n(\mathbf{k})$ have to be determined by accumulating photoelectrons over a sufficiently wide energy range, ideally being the entire conduction-band width. Despite the absence of quasiparticles and hence a discontinuity, there will still be an anomaly in $n(\mathbf{k})$ and consequently a maximum in $|\nabla_{\mathbf{k}} n(\mathbf{k})|$ at $\mathbf{k}_F$, facilitating the determination of a generalized FS.

We wish to thank J. Osterwalder (Zürich) and P. Aebi (Fribourg) for sharing with us the technology for Fermi surface mapping. We are also grateful to Z.-X. Shen (Stanford) for helpful discussions. This work was supported by the Deutsche Forschungsgemeinschaft (SFB 277 and Grant No. 149/17-1,2) and by the BMBF.

[1] N. W. Ashcroft and N. D. Mermin, *Solid State Physics* (Saunders College Publishing, Fort Worth, 1976).
[2] D. Shoenberg, *Magnetic Oscillations in Metals* (Cambridge University Press, Cambridge, 1984).
[3] A. Santoni *et al.*, Appl. Phys. A **52**, 299 (1991); R. L. Kurtz *et al.*, Nucl. Instrum. Methods Phys. Res. A **319**, 257 (1992); A. P. J. Stampfl *et al.*, Surf. Sci. **331–333**, 1272 (1995).
[4] J. Osterwalder *et al.*, in *Proceedings of the 10th Vacuum Ultraviolet Radiation Physics*, Paris, France, 1992, edited by F. J. Wuilleumier, Y. Petroff, and I. Nenner (World Scientific, Singapore, 1993); P. Aebi *et al.*, Surf. Sci. **307–309**, 917 (1994).
[5] P. Aebi *et al.*, Phys. Rev. Lett. **72**, 2757 (1995).
[6] P. Nozières, *Theory of Interacting Fermi Systems* (Benjamin, New York, 1964).
[7] R. Claessen *et al.*, Phys. Rev. B **54**, 2453 (1996).
[8] R. Claessen *et al.*, Phys. Rev. Lett. **69**, 808 (1992).
[9] J. W. Allen *et al.*, J. Phys. Chem. Solids **56**, 1849 (1995).
[10] R. Claessen *et al.*, Physica B (to be published).
[11] Th. Straub *et al.* (unpublished).
[12] A. R. Williams, J. Kübler, and C. D. Gelatt, Jr., Phys. Rev. B **19**, 6094 (1979).
[13] N. V. Smith and M. M. Traum, Phys. Rev. B **11**, 2087 (1975).
[14] C. O. Almbladh and L. Hedin, in *Handbook on Synchrotron Radiation*, edited by E. E. Koch (North-Holland, Amsterdam, 1983), Vol. 1b.
[15] M. Randeria *et al.*, Phys. Rev. Lett. **74**, 4951 (1995).
[16] J. C. Campuzano *et al.*, Phys. Rev. B **53**, R14 737 (1996).
[17] The effective **k** broadening Δk is determined by the angular reso-

lution of the analyzer through $\Delta k_\theta = 0.512\sqrt{E_{\rm kin}}\cos\theta\Delta\theta$ and athermal contribution resulting from a nonzero width of the Fermi-Dirac distribution at finite T, which can be estimated by $\Delta k_T = 4k_B T \cdot v_F^{-1}$, where v_F is the Fermi velocity. For our measurement on Cu this amounts to $\Delta k \approx 0.15$ Å^{-1}.

[18] P. Thiry *et al.*, Phys. Rev. Lett. **43**, 82 (1979).

[19] P. T. Coleridge and I. M. Templeton, Phys. Rev. B **25**, 7818 (1982).

[20] Z. Qu *et al.*, Surf. Sci. **324**, 133 (1995).

[21] P. Aebi *et al.* (unpublished).

[22] J. Voit, Rep. Prog. Phys. **58**, 977 (1995).